Research Square

Preprints are preliminary reports that have not undergone peer review.
They should not be considered conclusive, used to inform clinical practice,
or referenced by the media as validated information.

Carbohydrate ProLectin-M, a Galectin-3 Antagonist, Blocks SARS-CoV-2 Activity

ALBEN SIGAMANI (dralbens@myrescon.com)
Research Consultancy India

Hana Chen-Walden
Pharmalectin, an Unit of Bioxytran Inc

Jayeeta Pahan
Murlikrishna Pharma Pvt Ltd

Michelle C. Miller
University of Minnesota

Kevin H Mayo
University of Minnesota

David Platt
Pharmalectin, an Unit of Bioxytran Inc

Article

Keywords:

Posted Date: April 20th, 2022

DOI: https://doi.org/10.21203/rs.3.rs-1531940/v1

License: This work is licensed under a Creative Commons Attribution 4.0 International License.
Read Full License

Abstract

The SARS-COV-2 (Severe Acute Respiratory Syndrome Coronavirus 2) virus binds to human lectins to gain entry into cells to replicate. Blocking the virus's entry using a complex polysaccharide component of pectin [α (1–6)- **D**-mannopyranose termed "ProLectin M" and Rhamnogalacturonan-II (RG-II)] that has an effect on viral replication as a therapeutic tool and a safe alternative to existing anti-viral therapies. Little is known about antagonizing galectin-3 viral-blocking activity by inhibiting viral entry into cells and subsequent viral replication, and its impact on the course of infection. Here, we investigated the effect of these non-cytotoxic polysaccharides on Vero cells infected with SARS-CoV-2 virus and demonstrated a dose-dependent reduction in viral load over a 48-hour incubation period with the virus. A pilot clinical study in five patients with laboratory-confirmed COVID-19 disease were treated with an oral formulation of α(1–6)-**D**-mannopyranose (ProLectin M). All patients achieved complete disease remission with zero hospitalisation or need for oxygen support. Moreover, viral load was significantly lowered within 2 days of drug administration. On the viral envelope, glycans often play a crucial role in enabling transmission of the pathogen and/or entry into its susceptible target cells. In this regard, our NMR spectroscopic studies showed on the molecular level that ProLectin M binds relatively strongly to galectin-3, supporting the idea of an antagonist effect on the lectin. Overall, our study demonstrates that blocking the viral envelope glycans can compromise entry of the virus into susceptible target cells that may translate into a positive clinical effect on the course of infection.

Introduction

Severe acute respiratory syndrome-associated coronaviruses infect human beings through aerosol transmission[1]. The Severe Acute Respiratory Syndrome Coronavirus 2 (SARS-CoV-2) virus has caused widespread infections, with the most recent variant of the virus being responsible for over 450 million cases and 6 million deaths globally[2]. Several vaccines have been approved[3] and after over 10 billion doses, the virus continues to spread and infect all age groups. SARS-CoV-2 has a unique nucleic acid structure, with its RNA coding for structural proteins that trap lectins that recognize host cell sugar chains and evade the host's immune defense system[4]. Glycosylation gives a 3-dimensionally stable structure to the protein, providing e.g. protection from proteases that would degrade viral proteins. Viruses evade the host's immune defense systems by adding sugar chains to their spike proteins[5], and in some cases gain easy entry into host cells by being trapped by lectins that recognize host cell sugar chains[6]. One of these lectins is galectin-3 (Gal-3).

Galectins are a class of proteins that bind β-galactosides. Human Gal-3 is a chimera-type galectin with a single carbohydrate recognition domain (CRD). Gal-3 is highly expressed in activated T lymphocytes (e.g. neutrophils, monocytes, macrophages, dendritic cells) and epithelial and endothelial cells and fibroblasts[7]. Expression of Gal-3 enhances cytokine expression (e.g. TNFα, IL-1β and IL-6) in immune cells[8] promoting the so-called cytokine storm syndrome in patients infected with SARS-CoV[9] that can result in systemic organ failure and death[10]. Relatedly, Gal-3 interacts with the virus to facilitate entry into

T-cells[11] and activate NF-κB dependent pathways that leads to this upregulation of cytokines[12], thus enhancing inflammation[13]. High levels of Gal-3 have been observed in patients with severe COVID-19 vis-à-vis milder disease[11,14]. Gal-3 antagonists significantly reduce cytokine levels thereby reducing inflammation in patients with COVID-19[14-16].

Structurally, Gal-3 has the usual galectin carbohydrate recognition domain (CRD), as well as a long, aperiodic N-terminal tail. The CRD has a β-barrel fold with a 6-stranded β-sheet folded (sugar binding S-face) onto an opposing 5-stranded β-sheet (the F-face). Moreover, the galectin CRD structure has been identified in the N-Terminal Domain (NTD) of coronaviruses[17,18], including a high degree of structural similarity with this domain in SARS-CoV-2, and like Gal-3, this domain in SARS-CoV-2 binds *N*-acetylneuraminic acid (Neu5Ac), which is essential for viral entry into cells. This correlation may help explain why Gal-3 inhibitors are effective at reducing SARS-CoV-2 entry into cells[19]. Nevertheless, there is a paucity of therapeutics to treat COVID-19, and therefore a clear need to develop other and more effective agents[20].

Materials & Methods

ProLectin M production

Galectin antagonist was produced in a GMP facility located in Pune, Maharashtra. ProLectin M (PL-M) formulation was prepared and sent to the *in vitro* lab facility in Hyderabad, India. Details of the facility and process are shared in the Supplementary information file. Briefly, PL-M is an oral chewable tablet containing guar gum with added flavouring agents and other excipients.

Cell lines, virus and reagents

A virus stock of SARS-CoV-2 a3i clade sourced from original isolation from an infected patient in India was prepared according to company standard protocols for intact virus enrichment https://www.thermofisher.com. The viral stock was prepared by infecting Vero 76 cells (ATCC, CRL-1587) until a cytopathic effect (CPE) was visible two days post-inoculation. Vero 76 cells were cultured in Dulbecco Minimal Essential Medium (DMEM) (Thermo Scientific, USA), supplemented with 2% (v/v) Fetal Bovine Serum (FBS) (Sigma-Aldrich, St. Louis, USA), and 50 µg/mL gentamicin (Gemini Bio-products, USA).

Cytotoxicity assay

Cell viability was determined using the MTT [3-(4,5-dimethylthiazol-2-yl)-2,5-diphenyltetrazolium bromide; Sigma-Aldrich] assay. Vero cells were plated in triplicate in 96 well culture plates and incubated at 37°C under 5% CO_2. After reaching 90–95% cell confluency, different concentrations of PL-M were added to the cells for 24 hours to assess the cytotoxic effect on these cells. After 24 hours, 100 µL of MTT substrate (final concentration 50 µg/mL) was added to the cells, and the plate was incubated for 3 hours at 37ºC under 5% CO_2. Later, the formed formazan crystals were dissolved in 100 µL DMSO, and a multimode

microplate reader, Synergy HI (Agilent Technologies Inc., USA), was used to measure absorbance at 570 nm from which the percentage of viable cells was calculated.

Drug treatment

Vero cells were cultured in 96-well plates at 37°C under 5% CO_2 in DMEM supplemented media with 10% (v/v) FBS and 3.7 g/L sodium bicarbonate. At 90–95% confluency, cells were primed with a complete medium containing different concentrations of PL-M for 2 hours. The wells containing the test compound were replaced with the virus (~ MOI 0.1) in DMEM culture media (without FBS) for 3 hours. Later, the virus-containing medium was aspirated and replaced with fresh DMEM containing 10% FBS and test compound. Culture supernatant was collected for real time-PCR analysis of viral RNA copy.

Viral RNA extraction

Viral RNA was extracted from 200 µL aliquots of culture supernatants using the MagMAXTM viral/pathogen extraction kit (Applied Biosystems, Thermo Scientific). Viral supernatants from the test groups were mixed with a lysis buffer containing 260 µL of MagMAXTM viral/pathogen binding solution, 10 µL of MVP II binding beads, and 5 µL of MagMAXTM viral /pathogen proteinase-K for a total of 200 µL of sample in a deep well plate (KingFisherTM, Thermo Scientific). RNA extraction was performed using a KingFisher Flex system (version 1.01, Thermo Scientific) according to manufacture's instructions. The eluted RNA was stored at -80^{o}C until used.

RT-qPCR for detection of SARS-CoV-2

Quantitative PCR was performed using a Meril Covid-19 one step Real-Time PCR kit to detect the ORF1ab (FAM labeled) and nucleoprotein N (HEX labeled) genes of SARS-CoV-2 in the isolated RNA samples. Reaction conditions were set up according to manufacturer's protocol: 15 min at 50ºC (reverse transcription), 3 min at 95ºC (cDNA initial denaturation) followed by 15 sec at 95ºC (45 cycles of denaturation), 40 sec at 55ºC (annealing, extension and fluorescence measurement), and 10 sec at -25ºC (cooling). The program was set up using a QuantStudio-5 instrument (Thermo fisher). The threshold cycle (Ct) values of N gene (gene specific to SARS-CoV-2) were considered when plotting the graphs.

Anti-viral assay

To determine anti-viral effects from PL-M against SARS-CoV-2, Vero cells were first treated with various concentrations of the test compound. After 2 hours, the compound in the culture medium was removed, and viral stock (~ MOI 0.1 in DMEM culture media without FBS) was used to infect Vero cells at 37°C for 3 hours. The unabsorbed virus in the culture medium was then removed, and cells were washed and overlaid with 1 mL of fresh DMEM containing 10% FBS and test compound. After 48 hours, the viral supernatant was collected, and qRT-PCR was used to determine the reduction in viral RNA copy number as previously described. Uninfected Vero cells and those infected with viral stock were used as cell and infection controls, respectively.

For these experiments, two protocols were used. In Protocol 1, Vero cells on the plate were initially treated with PL-M prior to being infected with SARS-Cov-2 (DMSO was used as the control). In Protocol 2, Vero cells were initially cultured with the SARS-CoV-2 virus prior to being treated with drug-spiked media. FBS was used as the control.

Cells released from and bound to SARS-CoV-2 virus were analyzed to calculate the half-maximal effective concentration (EC_{50}) and half-inhibitory concentration (IC_{50}) values of our test compound by plotting % viral reduction or viral presence vs. log concentration of the test compound.

All experiments were conducted in a Biosafety Level – 3 accredited laboratory as per standard operating principles of Good Laboratory Practices and in a facility approved by the Government of India and Department of Science and Technology affiliated facility. No laboratory personnel were exposed more than expected risk in carrying out our experiments.

NMR Spectroscopy

Uniformly ^{15}N-labeled galectin-3 (Gal-3) was dissolved at a concentration of 20 μM in 20 mM potassium phosphate buffer at pH 6.9, made up using a 95% H_2O/ 5% D_2O mixture. ^{1}H-^{15}N HSQC NMR experiments were performed to investigate binding of PL-M and its individual polysaccharide components (galactomannans AG and R) to Gal-3. ^{1}H and ^{15}N resonance assignments for recombinant human Gal-3 were previously reported.[21]

NMR experiments were carried out at 30^{o}C on a Bruker 850 MHz spectrometer equipped with a H/C/N triple-resonance probe and an *x*/*y*/*z* triple-axis pulse field gradient unit. A gradient sensitivity-enhanced version of two-dimensional ^{1}H-^{15}N HSQC was applied with 256 (*t*1) x 2048 (*t*2) complex data points in nitrogen and proton dimensions, respectively. Raw data were converted and processed by using NMRPipe[22] and were analyzed by using NMRview[23].

Statistical analysis

PFU determined stock titers (ranging from Log10^{7}) were used to develop a regression equation and to calculate the percentage of viral reduction. After 72 hours of infection, the viral inhibition effect of the compound was assessed. The endpoint was calculated as the percentage of viral reduction using the following formula:

% Viral reduction = number of viral particles in infection control − number of viral particles exposed number of viral particles in infection control

The experiment was repeated twice, and results were averaged to calculate % viral reduction. The regression equation for viral particles vs. Ct value of the N- gene specific to SARS-CoV-2 virus (y = 3.5422x + 40.786; R2 = 0.99, x = viral particle number, and y = Ct value).

The number of viral particles calculated as

X = (40.786 – Ct Rd/Rp-genes at different time points)/3.5422.

The log reduction in % viral particles was interpreted as the efficacy of test compound in blocking viral infectivity in Vero cells. The student t-test was used to compare data to the control, and all data are presented as the mean ± SD.

Results

Anti-viral assay

Anti-viral assays (protocols 1 and 2 for pre- and post-treatment, respectively) with SARS-CoV-2 showed that PL-M render a nearly 99 percent (i.e. 2 log) reduction in viral RNA copy number compared to control (Figs. 1a-f, and Table 1). Pre-treatment (protocol 1) and post-treatment (protocol 2) of Vero cells with PL-M reduced viral load > 90%, i.e. from 7 µg/mL to 10 µg/mL, with the greatest reductions being observed before (94.4%) and after (59.7%) treatment with PL-M at doses of 8 µg/mL and 9 µg/mL, respectively. Viral particles were reduced from $10^{6.9}$ to $10^{5.1}$ and from $10^{6.9}$ to $10^{5.5}$ before and after PL-M treatment, respectively (Figs. 1a-f).

Table 1
Anti-SARS-CoV-2 effects of PL-M in pre-treated (Protocol 1) and post-treated (Protocol 2) Vero cells.

Protocol	Experimental	Treatment (µg/ml)	ProLectin-M
			Viral load reduction (%)
Protocol 1	Vero cells on a plate first treated with the drug before being infected with SARS-CoV-2/ control (DMSO)	1.0	38.41 ± 3.62
		3.0	73.33 ± 5.52
		4.0	80.92 ± 1.01
		5.0	79.94 ± 2.99
		6.0	83.16 ± 3.11
		7.0	93.03 ± 5.69
		8.0	94.37 ± 4.50
		9.0	93.26 ± 5.96
		10.0	92.26 ± 5.23
			Viral presence (%)
Protocol 2	Vero cells cultured with the SARS-CoV-2 virus before being treated with drug-spiked medium/ control medium (FBS)	0.5	87.63 ± 7.56
		3.0	81.30 ± 1.52
		4.0	53.78 ± 5.32
		5.0	58.45 ± 7.71
		7.0	42.19 ± 9.53

Values represent mean ± SD from triplicate analysis.

Protocol	Experimental	Treatment (µg/ml)	ProLectin-M
		8.0	43.48 ± 9.78
		9.0	40.32 ± 7.0
Values represent mean ± SD from triplicate analysis.			

Table 1:

Cytotoxic effect from PL-M on Vero cells

The MTT assay demonstrated that PL-M does not exhibit cytotoxic effects on Vero cells at concentrations up to 100 µg/mL, with CC_{50} values being > 100 µg/mL (Supplementary Fig. 1). In fact, the compound appeared to increase cell viability, with maximal effects from PL-M on cell proliferation observed at doses of 50 µg/mL (122.31 ± 0.10%) when compared to control (100%).

Binding of PL-M to Gal-3

Because PL-M reduces SARS-CoV-2 viral load and resolves clinical symptoms in patients[24], we hypothesized that PL-M functions *in situ* by binding to and antagonizing Gal-3 that normally interacts with SARS-CoV-2 to promote viral entry into cells[11]. To validate this proposal, we used NMR spectroscopy to assess interactions between PL-M and the lectin.

HSQC NMR spectra of ^{15}N-labeled Gal-3 (^{15}N-Gal-3) were measured as a function of PL-M concentration (0.3, 0.6, 1.2, 2.4 and 4.8 mg/mL). An ^{15}N-^{1}H HSQC spectral expansion is shown in Fig. 2a for ^{15}N-Gal-3 in the absence (peaks in black) and presence (peaks in red) of 1.2 mg/mL PL-M. During the titration, Gal-3 resonances are differentially chemically shifted and reduced in intensity (broadened), with some peaks becoming so broadened by the end of the titration that they cannot be observed. This observation alone demonstrates that Gal-3 binds to PL-M and indicates that the overall structure of Gal-3 is not significantly perturbed upon binding. Moreover, the fact that resonances are generally significantly broadened and minimally chemically shifted, PL-M binding to Gal-3 falls in the intermediate exchange regime on the chemical shift time scale, suggesting that the equilibrium dissociation constant (K_D) lies in the 2 µM to 100 µM range. The extent of resonance broadening is related to binding affinity and stoichiometry, in addition to any binding-induced changes in internal motions and conformational exchange. Therefore, one might look at this as binding avidity, or the net ability of PL-M to bind to Gal-3. Alternatively, the apparent broadening could result from multiple binding modes given the heterogeneous nature of the PL-M polysaccharide. Either way, Gal-3 binds to PL-M.

Even though PL-M binding-induced ^{15}N-Gal-3 chemical shift changes, Δδ, are relatively small, they are useful to assess where is the binding epitope on the lectin. Figure 2b plots ^{15}N-Gal-3 chemical shift changes, Δδ, vs. the amino acid sequence of Gal-3. The most shifted resonances arise from Gal-3 CRD

residues in β-strands 3, 4, 5 and 6 that comprise the S-face β-sheet of the β-sandwich to which the β-galactoside lactose binds, as illustrated in Fig. 2c that shows the structure of the Gal-3 CRD (pdb access code: 1A3K) with the most shifted residues being colour highlighted. This indicates that the PL-M binding epitope on Gal-3 is within the canonical sugar binding domain on the S-face of the CRD. Chemical shift changes within the N-terminal tail (NT) (residues 1-111) most likely result from PL-M binding-induced allosteric effects on the CRD F-face and modulation of interaction dynamics between the NT and CRD F-face[21]. Figure 2d plots chemical shift changes averaged over all Gal-3 resonances vs. the concentration of PL-M with the 50% saturation point in the plot falling at ~ 1 mg/mL. However, because Gal-3 binding falls in the intermediate exchange regime, one cannot accurately determine binding affinity/avidity (or stoichiometry), other than to say that the equilibrium dissociation constant, K_d, falls in the ~ 2 μM to ~ 100 μM range[25].

Discussion

Our results demonstrate viral blocking effects from PL-M that binds to Gal-3 and attenuates interactions between the galectin and the spike protein of the SARS-CoV-2 virus, thus reducing cell infectivity. PL-M is well tolerated (CC_{50} > 100 g/mL) by Vero cells and increased the number of viable cells, likely by stimulating cell proliferation. To assess viral entry blocking effectivity, Vero cells were infected with SARS-CoV-2 after and before treatment with PL-M according to protocols 1 and 2 (Table 1). In both instances, the study drug efficiently decreases viral load by an approximately 2 log reduction (≈ 99%) in viral RNA copy number as determined by RT-PCR (Figs. 1a-f). PL-M had excellent IC_{50} value of 6.18 μg/mL.

Our findings suggest that PL-M has significant viral blocking activity against SARS-CoV-2 via reduction of viral RNA replication. Several investigations have revealed that the sugar binding site on Gal-3 is crucial to function[26]. Inhibition of this site, particularly in Gal-3, may be one of the key mechanisms behind anti-SARS-CoV-2 action of the galactomannan polysaccharide, including our compound. Our NMR structural studies indicate that PL-M binds specifically to Gal-3 in the μM range. In relation to Gal-3 inhibitors, it is plausible that our compound interact with Gal-3 in the same way as does the structurally similar NTD of the S1 subunit of SARS-CoV-2. Overall, inhibition of Gal-3, as well as blockade of NTD of the S1 subunit and ACE2 receptors, may be prospective anti-SARS-CoV-2 actions of PL-M.

The SARS-CoV-2 manifested in COVID-19 (Coronavirus disease) has resulted in the recent global pandemic and concomitant economic hardship. In the absence of a clinically proven, effective anti-viral treatment, the COVID-19 virus has spread around the world, and further efforts are required to develop a safe and clinically effective anti-viral drug to combat this disease. Even though the use of vaccines is a proven intervention to combat many infections, including COVID[27], vaccines targeting the antigenic sites of spike protein have limited efficacy at inhibiting the spread of the virus. As the antigenic sites in the virus mutate, community spread of the virus can continue and global threats from these viruses are unlikely to go away[28]. In this regard, we need novel mechanisms to block their spread. Viruses bind to sugar chains on host cell membranes and mutations in these receptor binding proteins are less

frequent[29]. Sugar analogs or receptor sugar analogs that block the host cell sugar chains could potentially be used as drugs capable of overcoming viruses with mutagenic potential in their antigenic sites[30].

In conclusion, SARS-CoV-2 spike glycoprotein plays a key role in the virus's cellular attachment and entry processes. The S1-NTD of SARS-CoV-2 is structurally and sequentially similar to human Gal-3, which is crucial.

Data availability

All data supporting this study are provided in the main article, supplementary information files, and upon request to the corresponding author.

Abbreviations

Gal-3, galectin-3; PLM, ProLectin-M; PLI, ProLectin I; NMR, nuclear magnetic resonance spectroscopy; SARS-COV-2, Severe Acute Respiratory Syndrome Coronavirus 2.

References

1. Cui, J., Li, F. & Shi, Z.-L. Origin and evolution of pathogenic coronaviruses. Nature Reviews Microbiology **17**, 181–192 (2019).
2. Mousavizadeh, L. & Ghasemi, S. Genotype and phenotype of COVID-19: Their roles in pathogenesis. J Microbiol Immunol Infect **54**, 159–163, doi:10.1016/j.jmii.2020.03.022 (2021).
3. Khandia, R. *et al.* Emergence of SARS-CoV-2 Omicron (B.1.1.529) variant, salient features, high global health concerns and strategies to counter it amid ongoing COVID-19 pandemic. Environ Res **209**, 112816, doi:10.1016/j.envres.2022.112816 (2022).
4. Gong, Y., Qin, S., Dai, L. & Tian, Z. The glycosylation in SARS-CoV-2 and its receptor ACE2. Signal Transduction and Targeted Therapy **6**, 396, doi:10.1038/s41392-021-00809-8 (2021).
5. Casalino, L. *ACS Cent. Sci.* **6**, doi:10.1021/acscentsci.0c01056 (2020).
6. Gobeil, S. M. C. Science, doi:10.1126/science.abi6226 (2021).
7. Díaz-Alvarez, L. & Ortega, E. The Many Roles of Galectin-3, a Multifaceted Molecule, in Innate Immune Responses against Pathogens. *Mediators Inflamm* 2017, 9247574, doi:10.1155/2017/9247574 (2017).
8. Sato, S., St-Pierre, C., Bhaumik, P. & Nieminen, J. Galectins in innate immunity: dual functions of host soluble beta-galactoside-binding lectins as damage-associated molecular patterns (DAMPs) and as receptors for pathogen-associated molecular patterns (PAMPs). Immunol Rev **230**, 172–187, doi:10.1111/j.1600-065X.2009.00790.x (2009).
9. Zhang, C., Wu, Z., Li, J. W., Zhao, H. & Wang, G. Q. Cytokine release syndrome in severe COVID-19: interleukin-6 receptor antagonist tocilizumab may be the key to reduce mortality. Int J Antimicrob

Agents **55**, 105954, doi:10.1016/j.ijantimicag.2020.105954 (2020).

10. England, J. T. *et al.* Weathering the COVID-19 storm: Lessons from hematologic cytokine syndromes. Blood Rev **45**, 100707, doi:10.1016/j.blre.2020.100707 (2021).
11. Wang, J., Jiang, M., Chen, X. & Montaner, L. J. Cytokine storm and leukocyte changes in mild versus severe SARS-CoV-2 infection: Review of 3939 COVID-19 patients in China and emerging pathogenesis and therapy concepts. J Leukoc Biol **108**, 17–41, doi:10.1002/jlb.3covr0520-272r (2020).
12. Okamoto, M., Hidaka, A., Toyama, M. & Baba, M. Galectin-3 is involved in HIV-1 expression through NF-κB activation and associated with Tat in latently infected cells. Virus Res **260**, 86–93, doi:10.1016/j.virusres.2018.11.012 (2019).
13. Zhou, W. *et al.* Galectin-3 activates TLR4/NF-κB signaling to promote lung adenocarcinoma cell proliferation through activating lncRNA-NEAT1 expression. BMC Cancer **18**, 580, doi:10.1186/s12885-018-4461-z (2018).
14. De Biasi, S. *et al.* Marked T cell activation, senescence, exhaustion and skewing towards TH17 in patients with COVID-19 pneumonia. Nat Commun **11**, 3434, doi:10.1038/s41467-020-17292-4 (2020).
15. Kalfaoglu, B., Almeida-Santos, J., Tye, C. A., Satou, Y. & Ono, M. T-Cell Hyperactivation and Paralysis in Severe COVID-19 Infection Revealed by Single-Cell Analysis. Front Immunol **11**, 589380, doi:10.3389/fimmu.2020.589380 (2020).
16. Liu, X. *et al.* Single-Cell Analysis Reveals Macrophage-Driven T Cell Dysfunction in Severe COVID-19 Patients. *medRxiv*, 2020.2005.2023.20100024, doi:10.1101/2020.05.23.20100024 (2020).
17. Tortorici, M. A. *et al.* Structural basis for human coronavirus attachment to sialic acid receptors. Nat Struct Mol Biol **26**, 481–489, doi:10.1038/s41594-019-0233-y (2019).
18. Behloul, N., Baha, S., Shi, R. & Meng, J. Role of the GTNGTKR motif in the N-terminal receptor-binding domain of the SARS-CoV-2 spike protein. Virus Res **286**, 198058, doi:10.1016/j.virusres.2020.198058 (2020).
19. Milanetti, E. *et al.* In-Silico Evidence for a Two Receptor Based Strategy of SARS-CoV-2. Front Mol Biosci **8**, 690655, doi:10.3389/fmolb.2021.690655 (2021).
20. Caniglia, J. L., Asuthkar, S., Tsung, A. J., Guda, M. R. & Velpula, K. K. Immunopathology of galectin-3: an increasingly promising target in COVID-19. *F1000Res* **9**, 1078, doi:10.12688/f1000research.25979.2 (2020).
21. Ippel, H. *et al.* Intra- and intermolecular interactions of human galectin-3: assessment by full-assignment-based NMR. Glycobiology **26**, 888–903, doi:10.1093/glycob/cww021 (2016).
22. Delaglio, F. *et al.* NMRPipe: a multidimensional spectral processing system based on UNIX pipes. J Biomol NMR **6**, 277–293, doi:10.1007/BF00197809 (1995).
23. Johnson, B. A. & Blevins, R. A. NMR View: A computer program for the visualization and analysis of NMR data. J Biomol NMR **4**, 603–614, doi:10.1007/BF00404272 (1994).

24. Sigamani, A. *et al.* Galectin antagonist use in mild cases of SARS-CoV-2; pilot feasibility randomised, open label, controlled trial. *medRxiv*, 2020.2012.2003.20238840, doi:10.1101/2020.12.03.20238840 (2020).
25. Williamson, M. P. Using chemical shift perturbation to characterise ligand binding. Prog Nucl Magn Reson Spectrosc **73**, 1–16, doi:10.1016/j.pnmrs.2013.02.001 (2013).
26. Di Lella, S. *et al.* When galectins recognize glycans: from biochemistry to physiology and back again. Biochemistry **50**, 7842–7857, doi:10.1021/bi201121m (2011).
27. Organization, W. H. *COVID-19 vaccine tracker and landscape*, 2022).
28. Harvey, W. T. *et al.* SARS-CoV-2 variants, spike mutations and immune escape. Nature Reviews Microbiology **19**, 409–424, doi:10.1038/s41579-021-00573-0 (2021).
29. Lam, S. D., Waman, V. P., Orengo, C. & Lees, J. Insertions in the SARS-CoV-2 Spike N-Terminal Domain May Aid COVID-19 Transmission. *bioRxiv*, 2021.2012.2006.471394, doi:10.1101/2021.12.06.471394 (2021).
30. Lee, Y.-K. *et al.* Carbohydrate Ligands for COVID-19 Spike Proteins. Viruses **14**, doi:10.3390/v14020330 (2022).

Figures

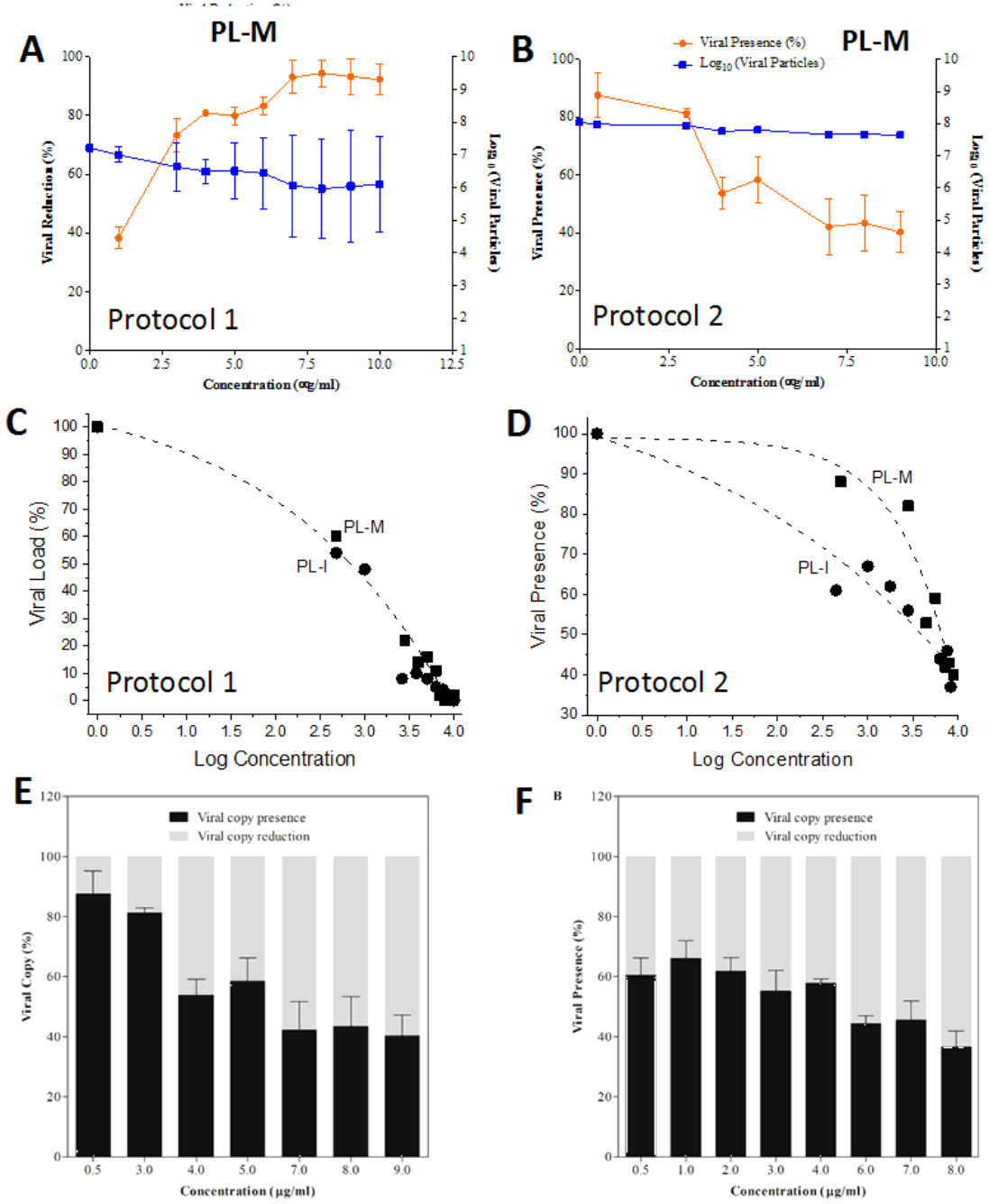

Figure 1

Anti-SARS-CoV2 efficacy of PL-M.

a Protocol 1: Reduction of viral load (circles) and viral particles (log_{10}, squares) in Vero cells pre-treated with PL-M. **b** Protocol 2: Reduction of viral load (circles) and viral particles (log_{10}, squares) in Vero cells pre-treated with PL-M. **c** Non-linear regression curves showing the reduction of viral load as a function of

PL-M (squares) Protocol 1. For PL-M, EC_{50} and EC_{90} values (which are essentially the same) are 1.53 and 9.26 µg/mL, respectively. **d** Non-linear regression curves showing the reduction of viral presence as a function of PL-M (squares) concentrations using Protocol 2. For PL-M, IC_{50} = 6.18 µg/mL. **e,f** Bar graphs showing percentage of viral copies (black bars) and viral copy reduction (grey bars) using PL-M.

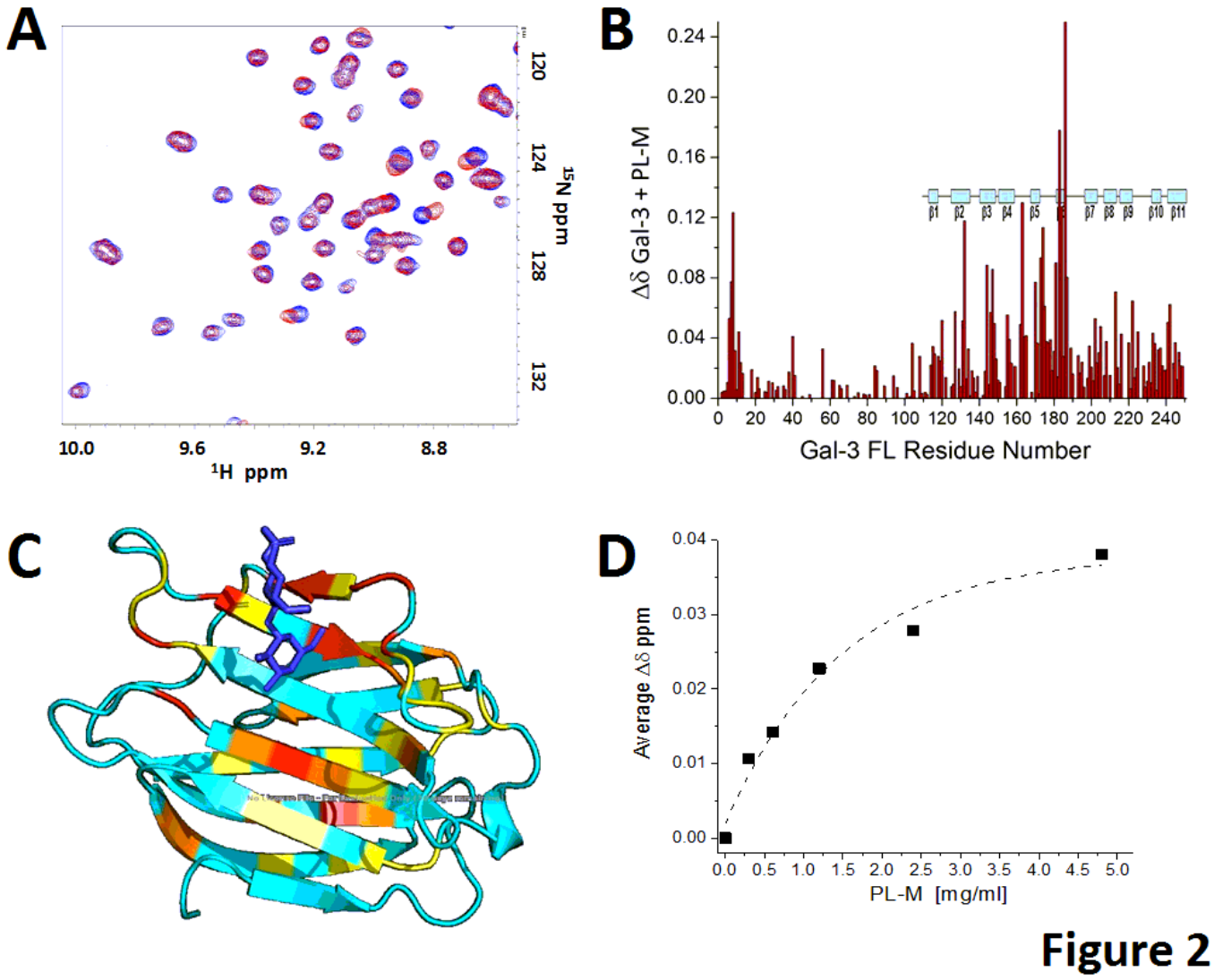

Figure 2

Figure 2

PL-M binding to Gal-3.

a ^{15}N HSQC expansions are overlaid for ^{15}N-labeled Gal-3 (20 mM) in the absence (black peaks) and presence of 1.2 mg/ml PL-M (red peaks). **b** Chemical shift map (Dd vs. the amino acid sequence of Gal-3) is shown for the binding of PL-M to Gal-3. Chemical shifts were internally referenced to DSS (4,4-dimethyl-4-silapentane-1-sulfonic acid), and chemical shift differences (Dd) were calculated as $[(D^1H)^2 + (0.25\ D^{15}N)^2]^{1/2}$. Solution conditions were 20 mM potassium phosphate, pH 6.9. **c** The crystal structure of the Gal-3 CRD (pdb access code: 1A3K; Seetharaman et al., 1998) is shown with the largest Dd values

highlighted in red (> 2SD above the Dd average), orange (between 1SD to 2SD above the Dd average), yellow (between the average and 1SD above the Dd average), and aqua (below the Dd average). For orientation, a molecule of bound lactose is shown in dark blue in stick format. **d** Dd values averaged over all Gal-3 residues are plotted vs the concentration of PL-M. Data were exponentially fitted as shown by the dashed line.

Supplementary Files

This is a list of supplementary files associated with this preprint. Click to download.

- SupplementaryFilenewProLectinM.docx